Patient-specific atrial fibrillation simulation prediction depend on rhythm used for calibration

Caterina Vidal Horrach[1], Ovais Ahmed Jaffery[1], Ross J Hunter[2], Shohreh Honarbakhsh[2], and Caroline Roney[1]

[1] Queen Mary University of London, London, United Kingdom
[2] Barts Health NHS Trust, London, United Kingdom

Abstract

Personalised therapies using patient-specific models of atrial fibrillation (AF) can enhance treatment outcomes. Electroanatomic data collected during an ablation procedure can be used to calibrate patient-specific activation and repolarisation properties, which affect AF properties and therapy outcomes. However, it is unknown how calibration data rhythm, pacing location, and choice of calibration technique affects prediction. In this study, we aim to compare AF properties and predicted therapy responses for patient-specific models calibrated using electroanatomic mapping data collected at different pacing rates. Initially, six patients underwent electroanatomic mapping during catheter ablation therapy, with pacing from a catheter in the coronary sinus at cycle lengths of 250ms and 600ms. Personalised anatomical models were constructed and calibrated to conduction velocity maps at each of the pacing rates. Simulations of AF were performed and pulmonary vein isolation was applied. Across the simulation models, all of the 6 cases had a greater number of occurrences of rotational activity for the models calibrated to 250ms than models calibrated to 600ms. This was most evident in the inferior wall, which had an average of 1.33 number of occurrences per patient at 250ms and an average of 0.17 number of occurrences per patient at 600ms. Thus, AF properties depend on the pacing rate used for model calibration.

1. Introduction

Atrial Fibrillation (AF) is one of the most common cardiac arrythmias worldwide. At present, ablation strategies in AF utilise a one size fits all approach where anatomical targets, such as pulmonary vein isolation, have been the main focus. However, the current success rate of catheter ablation therapy for AF is suboptimal, with several anatomical based approaches failing to improve on the success rate, with a recurrence rate of around 40% [1]. Approaching AF ablation by targeting substrate and electrophysiological changes will allow for a more personalised approach that is patient specific, with the potential to improve outcomes.

However, it is challenging to utilise data on the atrial substrate and electrophysiology to understand AF mechanisms and to determine optimal treatment approaches. Personalised computational models provide a framework to integrate these datasets, by including the effects of personalised anatomy, conduction velocity, restitution properties, and AF remodelling in a model that can be used to investigate patient-specific AF mechanisms and test treatment response.Thus, utilizing clinical patient-specific data and personalised modelling has the potential to revolutionise the management of AF, offering a more precise and efficient guide for treatment and prediction of AF.

However, it is unknown how best to personalise and calibrate these computational models, in part because the effects of rhythm on conduction properties is complicated. For example, Qureshi et al demonstrated that electroanatomic voltage maps vary with atrial rhythm, potentially revealing different types of fibrotic remodelling [2]. According to King et al., low CV is associated with increased risk of wavefront re-entry, resulting in possible initiation of an arrhythmia [3]. Additionally, regions of tissue with low CV often present as a more diseased state, possibly caused by fibrosis or changes in cell-to-cell coupling resulting in decreased connectivity [4]. In this study, we aimed to compare AF properties and predicted therapy responses for patient-specific models calibrated using electroanatomic mapping data collected at different pacing rates. This will offer insight into how calibration data rhythm, pacing location, and choice of calibration technique affects prediction.

2. Methods

We analysed clinical recordings, produced personalised anatomical models, and calibrated these personalised models to different pacing rates. We then simulated atrial fib-

rillation pre and post ablation. Finally, we analysed AF properties and predicted therapy responses at different pacing rates. A workflow of our methodology can be seen in Figure 1.
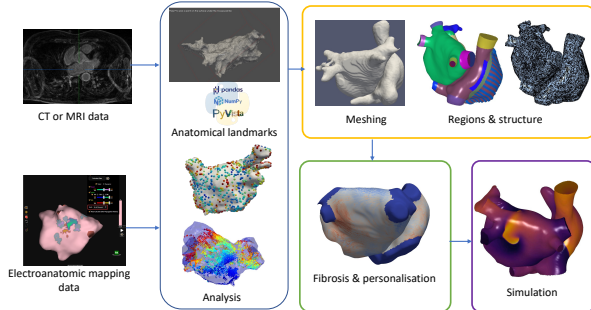

Figure 1. Overview of model construction pipeline.

2.1. Clinical Recordings

Patients undergoing catheter ablation for persistent AF at Barts Health NHS Trust were included in this study. All patients had persistent AF for less than 24 months. All patients granted permission to be involved in the study, which was approved by the UK National Research Ethics Service (22/PR/0961). The study was certified on clinicaltrials.gov (NCT05633303). Procedures on patients were carried out under conscious sedation or under general anaesthesia as per the clinical guidelines and the patient's choice. All procedures were executed on continuous anticoagulation therapy with heparin administration during the procedure to sustain an activated clotting time (ACT) of > 300 seconds. For each patient, high-density local activation time (LAT) maps were collected using the EnsiteX electroanatomic mapping system (Abbott) with the HD-grid catheter, with pacing from the coronary sinus (CS) at two different pacing intervals (PI). The PI chosen were 600ms, which represents a rate close to sinus rhythm, and 250ms, which represents a rate close to AF frequency.

2.2. Calculating Conduction Velocity

Conduction velocity (CV) was measured for each LAT map, which included an LA anatomical mesh and LATs at recording locations estimated to the atrial surface. For each map, we calculated CV using a gradient-based method. Each geometry was firstly re-meshed to a resolution of 2 mm utilising Meshtool software [5], and all calculations were executed on this mesh to minimize the impact of spatial resolution when differentiating results throughout the cases. An LAT was generated for each node on the mesh using interpolation of LAT readings. This was carried out using Meshtool software which applies an inverse distance

weighting interpolation. Thus, by measuring the distance between each element, the gradient of the interpolated LAT was utilized to estimate CV for each element of the mesh. The gradient was calculated using the MATLAB trigrad function, then the spatial gradient was inverted to estimate CV.

2.3. Producing anatomical models from electroanatomic data

The files extracted from the EAM system are analysed using a custom Matlab script which plots the clinical geometry of the left atrium to analyse the structure of the mesh and connectivity. This mesh is imported into Paraview for clipping, where the pulmonary veins (PVs) and the mitral valve (MV) are clipped. A python script was developed in order to select landmark coordinates for the left atrium by using the Pyvista library [6]. The mesh produced in the previous step is used to select the landmark points for the 4 PVs, the MV, LA Appendage, LA lateral wall, septal wall, and the right superior pulmonary vein (RSPV) and left superior pulmonary vein (LSPV) junctions. A universal atrial coordinate (UAC) system is required in order to register data between cases, and to add fibres to our anatomical models [7]. The UAC system maps a surface mesh of the left atrium to the unit square, permitting mapping of atlases and registration of geometries. This system is calculated by solving Laplace's equation on the geometry with Dirichlet boundary conditions of zero or one across the boundary nodes calculated using the landmarks. This was computed using openCARP and python scripts.

2.4. Calibrating Conduction Velocity Models

CV measurements were mapped to conductivity values in the monodomain equation. Firstly, a knnsearch pipeline was used to map the CV recording locations on the clinical mesh to the high resolution simulation mesh (0.2-0.3mm), assigning a CV value to each element of the simulation mesh. Distinct conductivity regions were included in the meshes based on 9 pre-computed CV - conductivity mappings. The 9 conductivity areas were included in the mesh via labels on each element. Conductivity values were then assigned in the simulation depending on the element labels to produce regions of different CV.

2.5. Processing pre and post ablation simulations

Pre-ablation and post-ablation simulations were run to analyse the differences in wavefront propagation and conduction velocity for models calibration to different PIs

(CS250ms and CS600ms) by calculating phase singularity maps. The simulations were run in openCARP [8] using the Courtemanche et al. ionic cell model [9] with the monodomain model for tissue propagation. The ionic properties in the Courtemanche et al. cell model were altered to represent physiological heterogeneity across the left atrium regions [10]. In the post-ablation simulations, pulmonary vein isolation (PVI) was simulated in each personalised calibrated model after 5s of AF. The PVI lesions were defined by a threshold distance between the LA body and the pulmonary veins. The PVI lesions applied were assigned as non-conductive when running the simulation. Both different types of simulations were run for each case and for the model calibrated to the different PIs (CS250ms, CS600ms). Post-PVI simulations were run for a total of 2s.

2.6. Post-Processing Simulation Data

To compare arrhythmia dynamics between models calibrated to the two PI, we post-processed transmembrane potential data using previously published phase mapping algorithms [11]. Specifically, for each model, we calculated the number of rotational drivers and areas of wavefront break-up across the LA by considering the distribution using a 6-segment anatomical model (LA segments: roof, anterior, lateral, septum, posterior and inferior). We used the following definitions: rotational drivers were specific regions or areas where a spiral wave is observed [12]; areas of wavefront break up were specific regions or areas where a wavefront divides into multiple wavefronts [13].

3. Results and Discussion

We analysed the relationship between rotational driver burden and pacing rate used for model calibration. On average the number of occurrences of rotational activity was higher for the 6 personalised anatomical models calibrated to 250ms pacing rate than for 600ms (5 and 2.5 respectively); an example is shown in Figure 2. Across the simulation models, all of the cases had a greater number of occurrences of rotational activity for the models calibrated to 250ms than the model calibrated to 600ms. The remaining cases demonstrated the same number of occurrences of rotational activity for the pacing rates.

In all regions of the LA, the models calibrated to a cycle length of 250ms had a higher number of rotational activities compared to the models calibrated to a cycle length of 600ms. This was most evident in the inferior wall, which had an average of 1.3 number of occurrences per patient for the model calibrated to 250ms, and an average of 0.17 number of occurrences per patient at 600ms. There was no rotational activity localized to the septal wall across any of the calibrated models; the findings above are shown in Figure 3A. Figure 3B shows a representation of the percent-
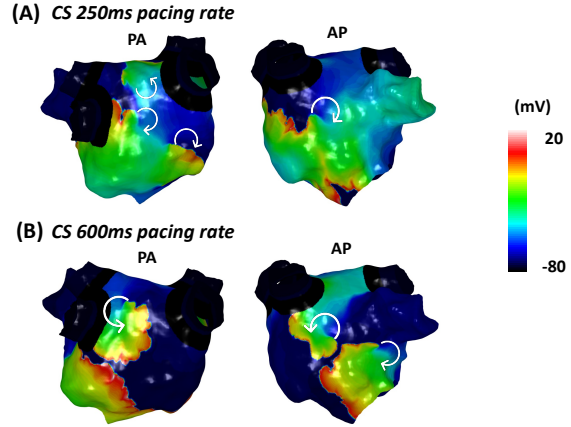

Figure 2. **Simulated propagation patterns post PVI for a model calibrated to two different pacing rates.** There is a visible difference in the number of rotational drivers between the pacing rate at 250ms (A), with fewer rotational drivers for calibration to 600ms pacing rate (B). Rotational arrows indicate rotational drivers, and straight arrows indicate planar wavefronts.

age of occurrences throughout the regions of the left atrium for the models calibrated to a pacing rates of 250ms and 600ms averaged across all personalised anatomical models. It also shows how the anterior wall has the highest percentage for both pacing rates, and the septum has the lowest percentage for both pacing rates.

Identifying the rotational driver distribution across the 6 anatomical segments of the LA allows us to determine and consider the impact of fixed scar tissue and functional remodelling on AF. Specifically, the two different pacing rates allow differentiation between fixed scar that is more likely to be observed at a PI of 600ms, and functional remodelling that may require a faster pacing rate (e.g. PI 250ms) to see the effects of restitution on electrical wavefronts [2].

4. Conclusion

AF properties depend on the pacing rate used for model calibration. Our future work will calibrate patient-specific restitution properties, and compare AF model patterns and predicted therapy outcomes to clinical recordings.

Acknowledgments
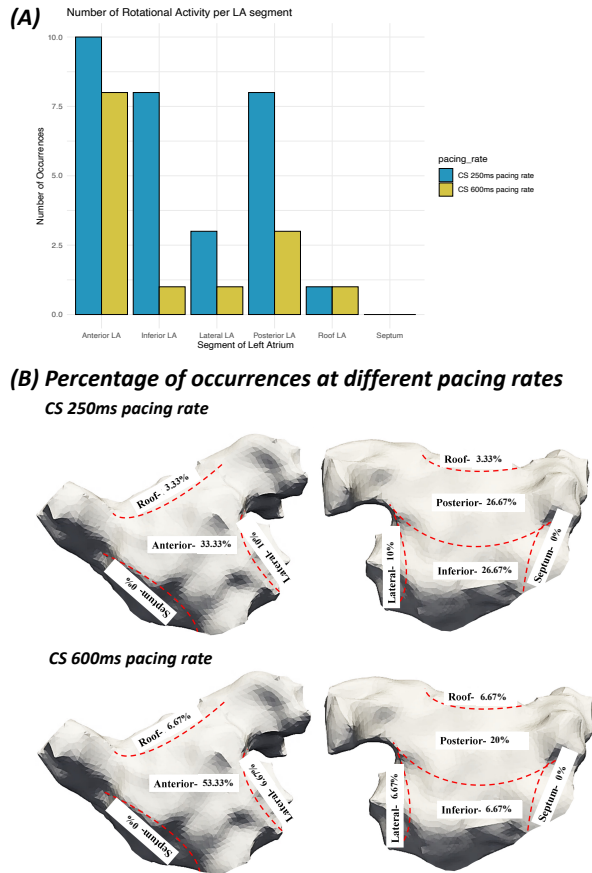
Figure 3. **Number of rotational drivers varies depending on the pacing rate used for calibration: Regional analysis.** (A) Total number of rotational occurrences in each LA anatomical segment for models calibrated to each pacing rate (250ms and 600ms). (B) Percentages of rotational activity for each calibrated model in the different LA anatomical segments.

References

[1] Chew DS, Black-Maier E, Loring Z, Noseworthy PA, Packer DL, Exner DV, Mark DB, Piccini JP. Diagnosis-to-ablation time and recurrence of atrial fibrillation following catheter ablation: a systematic review and meta-analysis of observational studies. Circulation Arrhythmia and Electrophysiology 2020;13(4):e008128.

[2] Qureshi NA, Kim SJ, Cantwell CD, Afonso VX, Bai W, Ali RL, Shun-Shin MJ, Malcolme-Lawes LC, Luther V, Leong KM, et al. Voltage during atrial fibrillation is superior to voltage during sinus rhythm in localizing areas of delayed enhancement on magnetic resonance imaging: an assessment of the posterior left atrium in patients with persistent atrial fibrillation. Heart rhythm 2019;16(9):1357–1367.

[3] King JH, Huang CLH, Fraser JA. Determinants of myocardial conduction velocity: implications for arrhythmogenesis. Frontiers in physiology 2013;4:154.

[4] Cantwell CD, Roney CH, Ng FS, Siggers JH, Sherwin SJ, Peters NS. Techniques for automated local activation time annotation and conduction velocity estimation in cardiac mapping. Computers in biology and medicine 2015; 65:229–242.

[5] Neic A, Gsell MA, Karabelas E, Prassl AJ, Plank G. Automating image-based mesh generation and manipulation tasks in cardiac modeling workflows using meshtool. SoftwareX 2020;11:100454.

[6] Sullivan CB, Kaszynski A. PyVista: 3d plotting and mesh analysis through a streamlined interface for the visualization toolkit (VTK). Journal of Open Source Software may 2019;4(37):1450. URL https://doi.org/10.21105/joss.01450.

[7] Roney CH, Pashaei A, Meo M, Dubois R, Boyle PM, Trayanova NA, Cochet H, Niederer SA, Vigmond EJ. Universal atrial coordinates applied to visualisation, registration and construction of patient specific meshes. Medical image analysis 2019;55:65–75.

[8] Plank G, Loewe A, Neic A, Augustin C, Huang YL, Gsell MA, Karabelas E, Nothstein M, Prassl AJ, Sánchez J, et al. The opencarp simulation environment for cardiac electrophysiology. Computer Methods and Programs in Biomedicine 2021;208:106223.

[9] Courtemanche M, Ramirez RJ, Nattel S. Ionic mechanisms underlying human atrial action potential properties: insights from a mathematical model. American Journal of Physiology Heart and Circulatory Physiology 1998; 275(1):H301–H321.

[10] Bayer JD, Roney CH, Pashaei A, Jaïs P, Vigmond EJ. Novel radiofrequency ablation strategies for terminating atrial fibrillation in the left atrium: a simulation study. Frontiers in physiology 2016;7:108.

[11] Roney CH, Cantwell CD, Qureshi NA, Chowdhury RA, Dupont E, Lim PB, Vigmond EJ, Tweedy JH, Ng FS, Peters NS. Rotor tracking using phase of electrograms recorded during atrial fibrillation. Annals of biomedical engineering 2017;45:910–923.

[12] Zaman JA, Rogers AJ, Narayan SM. Rotational drivers in atrial fibrillation: are multiple techniques circling similar mechanisms?, 2017.

[13] Kiyama T, Kanazawa H, Yamabe H, Ito M, Kaneko S, Kanemaru Y, Kawahara Y, Yamanaga K, Fujisue K, Sueta D, et al. Analysis of the driving mechanism in paroxysmal atrial fibrillation: comparison of the activation sequence between the left atrial body and pulmonary vein. Journal of Cardiology 2020;75(6):673–681.

Address for correspondence:

Caterina Vidal Horrach

Digital Environment Research Institute (DERI), Empire House, 67-75 New Road, London, E1 1HH, United Kingdom

caterina.vidalhorrach@qmul.ac.uk